

Article

Kinetics of Ion-Exchange Extraction of Lithium from Aqueous Solutions by Protonated Potassium Polytitanates

Maria Vikulova * , Lilia Maximova , Valeria Rudyh, Nikolay Gorshkov  and Alexander Gorokhovskiy

Department of Chemistry and Technology of Materials, Yuri Gagarin State Technical University of Saratov, 77 Polytechnicheskaya Street, 410054 Saratov, Russia

* Correspondence: vikulovama@yandex.ru; Tel.: +7-917-322-25-59

Abstract: In this work, protonated forms of potassium polytitanate were obtained by treating the precursor in HCl solution at pH 2.0, 3.0, 4.0, 5.0, 6.0, or 7.0. The synthesized materials were studied using XRD, FTIR, and XRF. The ion-exchange properties were studied using a LiCl solution with a concentration of $C(\text{Li}^+) = 0.01$ mol/L. It was shown that extraction of lithium by potassium polytitanates is dependent on their protonation degree. It has been established that the samples with the highest degree of protonation obtained at pH = 2.0 and 3.0 have the highest efficiency in the ion-exchange extraction of Li^+ ions from an aqueous solution. For determination of exchange ion rates and the mechanism of the ion-exchange process, pseudo-first- and pseudo-second-order models as well as the Weber–Morris intraparticle diffusion model, were employed. Experimental data with their participation are in good agreement with the pseudo-second-order kinetic model. The calculated kinetic parameters were $q_e = 0.47\text{--}0.52$ mmol/g and $k_2 = 0.25\text{--}0.43$, depending on the protonation degree of potassium polytitanate. The obtained experimental and calculated values of the sorption capacity were compared with the cation-exchange capacity of materials studied. According to the kinetics study, the mechanism of lithium adsorption by potassium polytitanates with a higher protonation degree is the ion-exchange chemical reaction. Low-cost protonated potassium polytitanates are promising to extract Li^+ ions from aqueous solutions with a low concentration, as confirmed by the analysis of the results.

Keywords: potassium polytitanate; protonation; lithium; ion exchange; kinetics



Citation: Vikulova, M.; Maximova, L.; Rudyh, V.; Gorshkov, N.; Gorokhovskiy, A. Kinetics of Ion-Exchange Extraction of Lithium from Aqueous Solutions by Protonated Potassium Polytitanates.

Processes **2022**, *10*, 2258. <https://doi.org/10.3390/pr10112258>

Academic Editors: Sergei Alexandrov, Valentina Zhukova, Arcady Zhukov and Valeria Rodionova

Received: 29 September 2022

Accepted: 31 October 2022

Published: 2 November 2022

Publisher's Note: MDPI stays neutral with regard to jurisdictional claims in published maps and institutional affiliations.



Copyright: © 2022 by the authors. Licensee MDPI, Basel, Switzerland. This article is an open access article distributed under the terms and conditions of the Creative Commons Attribution (CC BY) license (<https://creativecommons.org/licenses/by/4.0/>).

1. Introduction

Lithium is the lightest metal element and is currently widely used in batteries for portable electronic devices and electric vehicles. The release of lithium into the environment because of anthropogenic impacts, including the extraction of coal and oil, is several times higher than its entry into the hydrosphere as a result of natural weathering processes [1]. In addition to the increase in lithium emissions from mining activities, wastewater discharge is one of the main sources of lithium in the environment, especially in metropolitan areas [2]. High levels of lithium are detected in water and biota, including public and domestic wells and marine organisms in coastal areas [3,4]. Studies have shown that elevated lithium concentrations are toxic to aquatic organisms and humans [5,6].

In addition to coastal and urban environments [7,8], agroecosystems can suffer from lithium pollution. Lithium in soil solution is easily absorbed by plant roots [9] and bioaccumulates in various cultures [10,11]. Lithium not only causes a decrease in chlorophyll content and necrotic spots in plants [6,12], but also promotes trophic transfer, which poses a potential risk to animal and human health, i.e., high concentration of lithium can contribute to the development of tremor, edema, cardiac arrhythmia, disturbance in GIT, and hypothyroidism. The nervous, renal and endocrine systems in humans are most sensitive to lithium [9].

Adsorption and ion-exchange methods for lithium extraction from aqueous solutions have received the most widespread attention among researchers, primarily because of the possibility of adsorbent/ion-exchanger regeneration and its repeated use, as well as methods for lithium extraction from solutions with low concentrations to meet the demand for it in various areas [13–17].

Among the known adsorbents, compounds with the spinel structure of the composition Li–Mn–O have received the greatest interest for lithium extraction from water resources. A large number of different methods for their synthesis have been developed, and their adsorption or ion-exchange capacities for lithium extraction from different water resources vary from 0.2 to 8.0 mmol/g [18–30].

However, titanium oxide derivatives have the greatest prospects in lithium recovery processes due to their environmental friendliness, insolubility in acid, and greater stability compared to manganates in the lithium desorption process, which allows maintaining the high ion-exchange efficiency of the ion exchanger after regeneration. The most studied representative of this group of compounds in the field of lithium extraction is metatitanic acid (H_2TiO_3) [31–39]. The structure of the crystal lattice of hydrated titanium oxide determines its selectivity with respect to lithium ions in the presence of cations such as sodium, potassium, magnesium, and calcium ions.

An X-ray amorphous analog of titanium dioxide and alkali metal titanates is potassium polytitanate, which is a group of layered compounds with the general formula $\text{K}_2\text{O} \cdot n\text{TiO}_2$, where n varies with the synthesis conditions. In this work, in terms of chemical composition and stoichiometry, it is close to potassium tetratitanate $\text{K}_2\text{Ti}_4\text{O}_9$. Titanium–oxygen octahedrons form layers of various configurations, the negative charge of which is compensated for by potassium cations in the interlayer space. Potassium polytitanate, like other similar structures, can undergo a protonation process, i.e., replacing potassium ions with hydrogen ions [40–43]. The protonated forms of potassium polytitanate are similar in composition and structure to metatitanic acid and can become a more attractive alternative due to the simplicity and low cost of synthesis. At the same time, by adjusting the conditions for the protonation of potassium polytitanate, it is possible to vary the structural characteristics of the resulting protonated products, thereby obtaining ion exchangers of different efficiency.

Inorganic ion exchangers for lithium extraction from solutions of various compositions and concentrations are predominantly manganates or titanates with a spinel structure. They are synthesized using a lithium-containing precursor, which causes their high cost, and then subjected to the protonation process. These materials have a layered structure stabilized by lithium or hydrogen. In this work, for the first time, potassium polytitanate is as a raw material for obtaining an effective protonated form of an ion exchanger. Unlike crystalline analogs, the structural units of potassium polytitanate are connected at different angles, forming a semicrystalline layered structure. The octahedral framework includes continuous rows of interstices, where potassium ions are located together with H_2O molecules, which contributes to different local distances between the sheets and suggests their good ion-exchange and sorption characteristics. Previously, there has not been a comprehensive study of the effectiveness of protonated forms of potassium titanates as ion exchangers for the extraction of lithium from aqueous solutions. The study of the influence of the degree of substitution of potassium ions for hydrogen ions in their interlayer space on the ion-exchange capacity and stability of the structure during the ion-exchange process is of particular interest.

Thus, the aim of this work is the synthesis and study of the ion-exchange properties of potassium polytitanates with different degrees of protonation to Li^+ ions.

2. Materials and Methods

2.1. Samples Preparation

Prepared 0.1 M HCl (35%, Russian standard 3118-77, Vekton, Saint Petersburg, Russia) solution was added to an aqueous suspension of potassium polytitanate, synthesized according to the method [44], to pH 2.0, 3.0, 4.0, 5.0, 6.0, or 7.0, and left to mix for 2 h.

The samples were then dried and ground. Depending on the conditions of obtaining, the objects of study were named as PPTP2, PPTP3, PPTP4, PPTP5, PPTP6, and PPTP7. The cation-exchange capacity was estimated for $K_2O \cdot nTiO_2$ ($n = 4.3$). The theoretical cation-exchange capacity calculated from formulas was 4.83 mmol/g. The cation-exchange capacity (CEC) determined with 1 M NH_4Cl (99.5%, Russian standard 3773-72, Vekton, Saint Petersburg, Russia) was 3.43 mmol/g, while the external cation-exchange capacity (ECEC) determined using the method of Ming and Dixon was 0.42 mmol/g [45–47]. The concentration of K^+ was determined using a potentiometric method with a laboratory ion meter I-160MP (Gomel Plant of Measuring Instruments, Minsk, Republic of Belarus) with a potassium-selective electrode ELIS-121K (Izmeritelnaya Tekhnika, Moscow, Russia).

2.2. Samples Characterization

The chemical composition was determined using a BRA-135F spectrometer (BOUREVE STNIK, Saint Petersburg, Russia). XRD data were obtained using an ARL X'TRA device (Thermo Scientific, Ecublens, Switzerland) using Cu-K α radiation ($\lambda = 0.15412$ nm). The degree of crystallinity was determined using the WinXRD 2.1-1 Crystallinity version 1 software. A Fourier-transform infrared spectrometer FT-801 (Simex, Novosibirsk, Russia) was applied to analyze surface functional groups. Scanning electron microscope ASPEX Explorer (ASPEX, Framingham, MA, USA) was employed for morphological analysis. An Analysette-22 NanoTech laser particle size analyzer (Fritsch, Idar-Oberstein, Germany) was used to determine the particle size distribution.

2.3. Kinetics of Ion Exchange

A suspension of protonated potassium polytitanate ($D = 10$ g/L) was mixed with a LiCl solution (99.2%, TC 6-09-3751-838, Rushim, Moscow, Russia) with $C(Li^+) = 0.01$ mol/L. The total volume of the mixture was 100 mL. The pH of the mixtures was maintained at a level of 8.0 by adding an aqueous solution of NH_4OH (25%, Russian standard 3760-79, Sigma Tec, Moscow, Russia). The systems were stirred using a magnetic stirrer at room temperature, and the change in the concentration of Li^+ ions was recorded by a potentiometric method using a laboratory ion meter I-160MP (Gomel Plant of Measuring Instruments, Republic of Belarus) with a lithium-selective electrode ELIS-142Li (Izmeritelnaya Tekhnika, Russia) every 5, 10, 20, 30, 60, 90, 120, 150, 180, 210, and 240 min.

The extraction efficiency of Li^+ ions (E , %) and the ion-exchange capacity of protonated potassium polytitanates (q , mmol/g) were calculated using the following formulas:

$$E, \% = \frac{C_0 - C_t}{C_0} \times 100\%, \quad (1)$$

$$q, \frac{\text{mmol}}{\text{g}} = \frac{C_0 - C_t}{m} \times V, \quad (2)$$

where C_0 is the initial concentration of Li^+ ions in the solution (mmol/L), C_t is the concentration of Li^+ ions in the solution at time t (mmol/L), m is the mass of protonated potassium polytitanate (g), and V is the volume of the solution (L).

For determination of exchange ion rates, pseudo-first- (Equation (3)) and pseudo-second-order (Equation (4)) models were employed.

$$\ln(q_e - q_t) = \ln q_e - k_1 t, \quad (3)$$

$$\frac{t}{q_t} = \frac{1}{k_2 q_e^2} + \frac{t}{q_e}, \quad (4)$$

where q_e (mmol/g) and q_t (mmol/g) are the number of Li^+ ions subjected to ion exchange at equilibrium and at time t , respectively; k_1 (min^{-1}) and k_2 ($\text{g}/(\text{mmol min})$) are constants of pseudo-first- and pseudo-second-order kinetics, respectively.

For study of intraparticle diffusion processes, the Weber and Morris diffusion model was employed (Equation (5)).

$$q_t = Kt^{0.5} + C, \quad (5)$$

where K is the diffusion rate constant ((mmol/g)·min^{0.5}), and C is parameter related to the thickness of the boundary layer (mmol/g).

3. Results and Discussion

Protonation was carried out by treating the initial potassium polytitanate with a complex stoichiometry close to alkali metal tetratitanate (K₂Ti₄O₉) in a hydrochloric acid solution. As a result, an ion-exchange reaction of substitution of a part of the alkali metal for a hydrogen ion occurs:



The degree of substitution, which varied experimentally and was determined by the pH of the dispersion during protonation, was estimated from the data of X-ray fluorescence analysis (Table 1).

Table 1. Chemical composition and the degree of crystallinity of protonated potassium polytitanates.

Sample Name	Oxide Content (wt.%)		Empirical Formula	The Degree of Crystallinity (%)
	K ₂ O	TiO ₂		
PPTP2	10.4	89.6	K _{0.8} H _{1.2} Ti _{4.3} O _{8.5}	25.4
PPTP3	13.1	87.0	K _{1.0} H _{1.0} Ti _{4.3} O _{8.5}	21.9
PPTP4	14.2	85.8	K _{1.1} H _{0.9} Ti _{4.3} O _{8.5}	17.5
PPTP5	14.8	85.2	K _{1.2} H _{0.8} Ti _{4.3} O _{8.5}	16.9
PPTP6	15.0	85.0	K _{1.3} H _{0.7} Ti _{4.3} O _{8.5}	15.9
PPTP7	18.0	82.0	K _{1.5} H _{0.5} Ti _{4.3} O _{8.5}	10.3

An obvious pattern is traced to a decrease in the content of potassium and an increase in the content of hydrogen with a decrease in the pH of the dispersion during protonation.

The protonated samples are characterized by an X-ray amorphous structure, confirmed by the absence of pronounced narrow high-intensity reflections in X-ray diffraction patterns and the presence of a wide halo in the range $2\theta = 25\text{--}35^\circ$ (Figure 1). The observed broad reflections of low intensity refer to phases of titanium dioxide of various modifications. From Figure 1 using Bragg's equation, the interlayer distance is estimated at about 1.65 nm. The degree of crystallinity is in the range of 10–25.5% and decreases with increasing pH during the protonation of potassium polytitanate.

The study of the structure and identification of the functional groups of the obtained protonated forms of potassium polytitanates were carried out using the method of FTIR spectroscopy. The FTIR transmission spectra of the studied samples are characterized by the presence of several pronounced absorption bands (Figure 2).

The wide intense absorption band in the wavenumbers range of 3750–3000 cm^{−1} was attributed to stretching vibrations of hydroxyl groups, and it was found in the FTIR transmission spectra of all protonated potassium polytitanates. Deformation vibrations of physically adsorbed water or, according to some data, hydrogen ions appeared as an absorption band at 1630 cm^{−1}. It should be noted that, for the samples protonated in a strongly acidic medium (pH 2.0, 3.0, and 4.0), this band was more intense, which may confirm the different degree of protonation, increasing as the pH decreased during the protonation process. The two absorption bands at 1140 and 1050 cm^{−1} referred to bending vibrations of thianol groups, which were clearly visible in the FTIR spectra of potassium polytitanates obtained at pH 2.0, 3.0, and 4.0. In turn, samples kept at pH 5.0, 6.0, and 7.0 were characterized by more pronounced absorption bands responsible for the stretching vibrations of titanium–oxygen bonds.

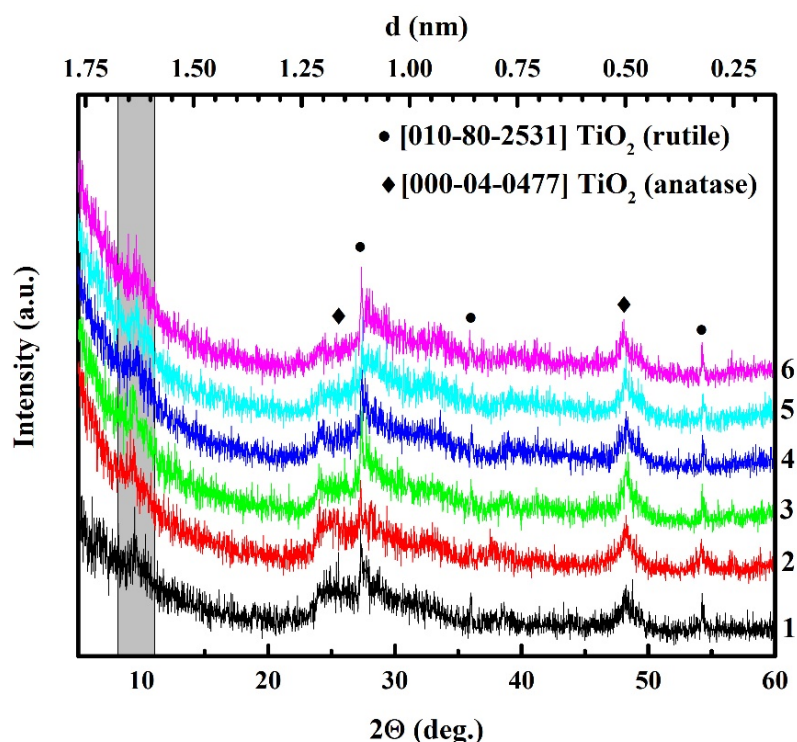


Figure 1. X-ray diffraction patterns of potassium polytitanates protonated under different conditions: pH 2.0 (1); pH 3.0 (2); pH 4.0 (3); pH 5.0 (4); pH 6.0 (5); pH 7.0 (6). The first peak corresponds to the interlayer distance.

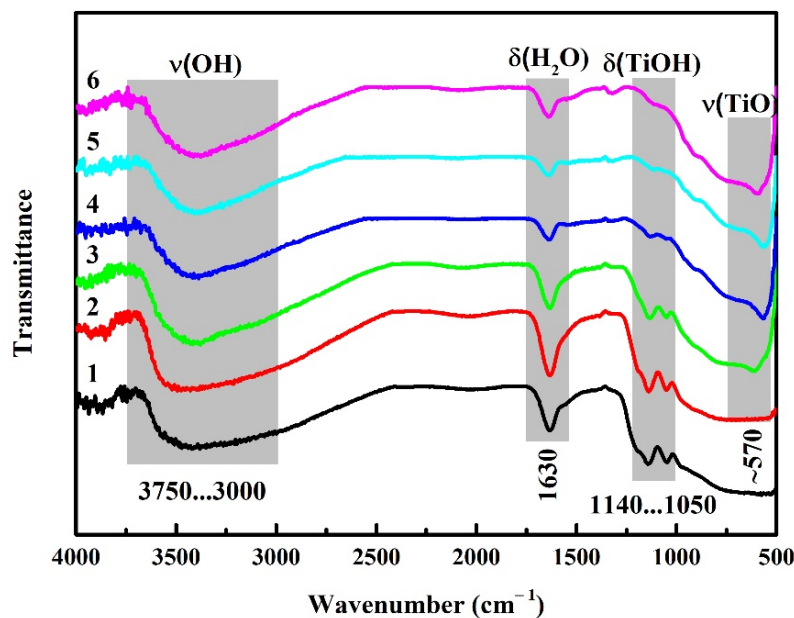


Figure 2. FTIR transmission spectra of potassium polytitanates protonated under different conditions: pH 2.0 (1); pH 3.0 (2); pH 4.0 (3); pH 5.0 (4); pH 6.0 (5); pH 7.0 (6).

Particles of protonated potassium polytitanates had a similar morphology, represented mainly by layered flakes forming agglomerates of various shapes and sizes. The gaps between individual particles and pores reached several micrometers (Figure 3).

According to the particle size distribution, the size of the agglomerates can vary on average from 3 to 20 μm . At the same time, the distribution was unimodal with small shoulders in the region of smaller sizes (Figure 4). The observed differences in

the sizes of agglomerates can be associated both with exfoliation processes occurring in acidic conditions and with the surface charge. Within the pH region of the suspension about the isoelectric point, the particle agglomeration occurs at a higher rate and complex agglomerates are formed, thereby resulting in a significant increase in the particle size [48]. The pH_{iso} of potassium polytitanate is about 6.6, which is why the particle size increased with increasing pH during the protonation process.

The efficiency of Li^+ ions extraction by potassium polytitanates with different degrees of protonation depending on the interaction time is shown in Figure 5.

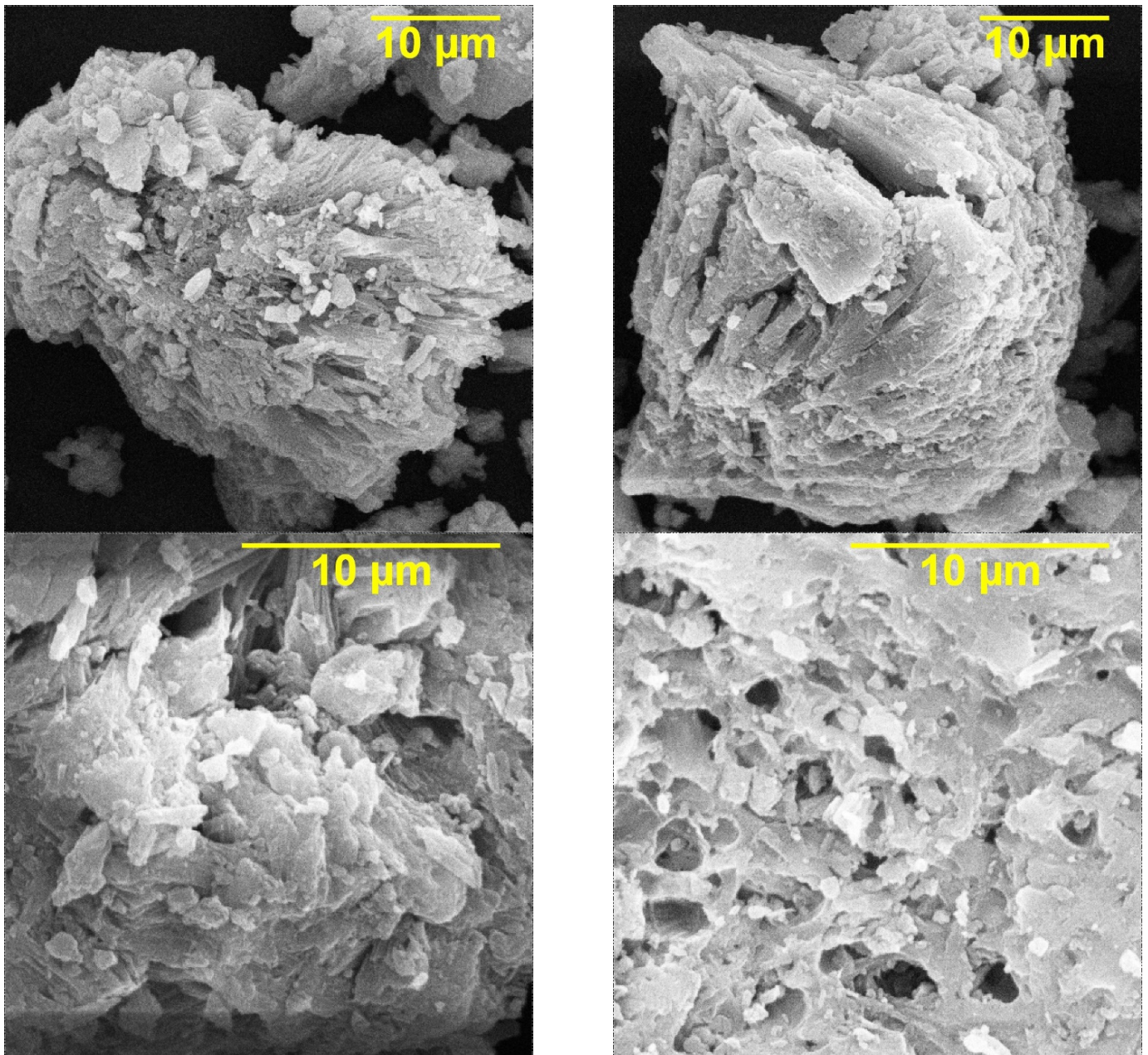


Figure 3. Scanning electron micrographs of particles of protonated potassium polytitanates.

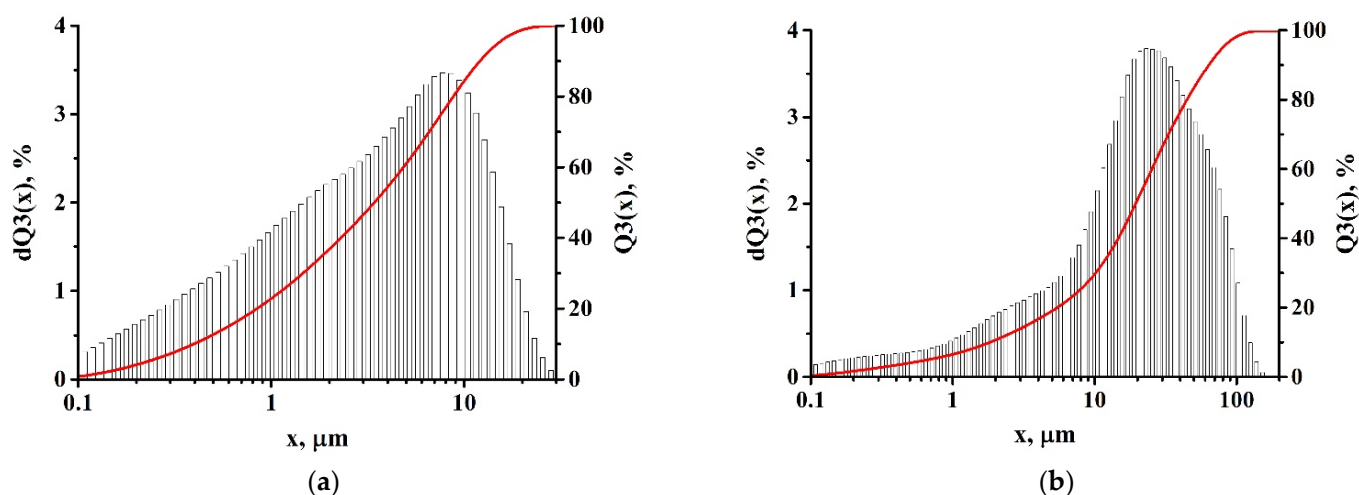


Figure 4. Particle size distribution of potassium polytitanates protonated at (a) pH 2.0 and (b) pH 7.0.

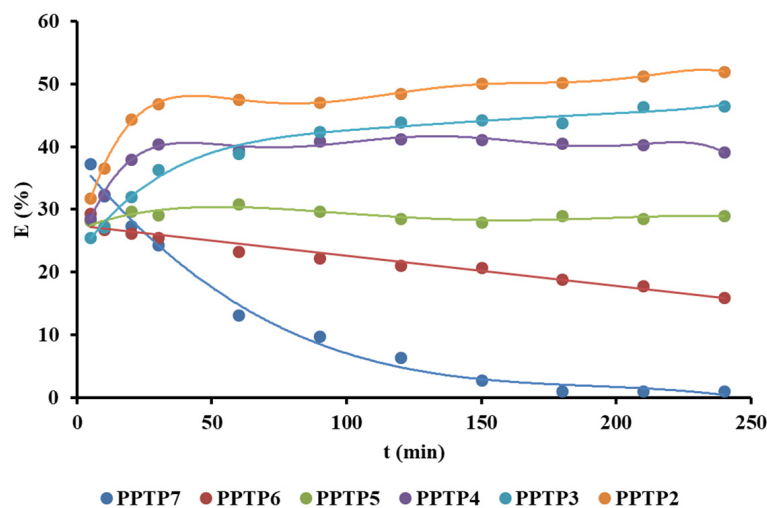
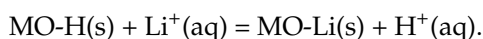


Figure 5. Efficiency of Li^+ ions extraction from an aqueous solution of LiCl with $C(\text{Li}^+) = 0.01 \text{ mol/L}$ by protonated potassium polytitanates, $D = 10 \text{ g/L}$, at room temperature.

Samples obtained at pH 7.0 and 6.0 demonstrated a decrease in the efficiency of Li^+ ions extraction with contact time. In the case of PPTP7, it was sharper; with the participation of PPTP6, it was less noticeable. As the pH decreased to ~ 5.0 during the protonation of potassium polytitanate, the compared index (E , %) was almost constant over the entire considered time range. A further decrease in the pH of the dispersion during the preparation of protonated forms of potassium polytitanate contributed to a change in the behavior of the curve and an increase in efficiency with an increase in the interaction time, reaching more than 50%. The revealed regularity can be explained by the different degree of protonation of the samples. In the case of potassium polytitanates with a high content of potassium ions, when potassium was replaced by lithium, the initial structure was destroyed, which led to the release of lithium into the solution. The isolated OH groups formed during protonation stabilized the structure and participated in the extraction of lithium. The action of ion exchangers was based on the following ion-exchange reaction [49]:



Therefore, a higher degree of protonation denotes a more efficient ion exchanger. This assumption was additionally confirmed by the decrease in the pH of the system after the ion-exchange process.

The ion-exchange process involving the samples with the highest efficiency (PPTP2 and PPTP3) was modeled using well-known pseudo-first- and pseudo-second-order chemical kinetics models, as well as the Morris–Weber intraparticle diffusion model.

Experimental data on the kinetics of Li^+ ion exchange with the participation of PPTP2 and PPTP3 are shown in Figure 6.

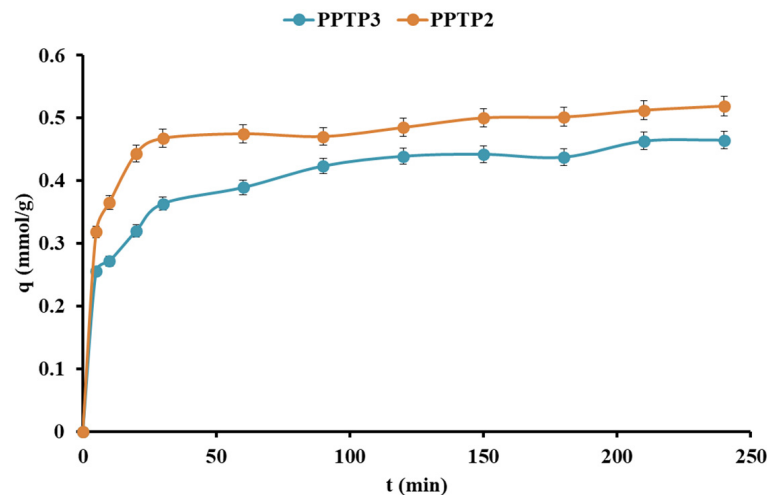


Figure 6. Kinetics of Li^+ ion exchange with the participation of PPTP2 and PPTP3 ($C(\text{Li}^+) = 0.01 \text{ mol/L}$, $D = 10 \text{ g/L}$, room temperature).

The kinetics of ion exchange was characterized by two distinct stages, i.e., a very fast one (during the first 20–30 min), followed by a slow one until the moment of saturation of the ion-exchange centers of the PPTP.

According to the correlation coefficient of linear regression (R^2 values), the experimental data on ion exchange better fit the pseudo-second-order model, which indicates the applicability of this model to the description of the mechanism of interaction of protonated potassium polytitanates with Li^+ ions (Figure 7).

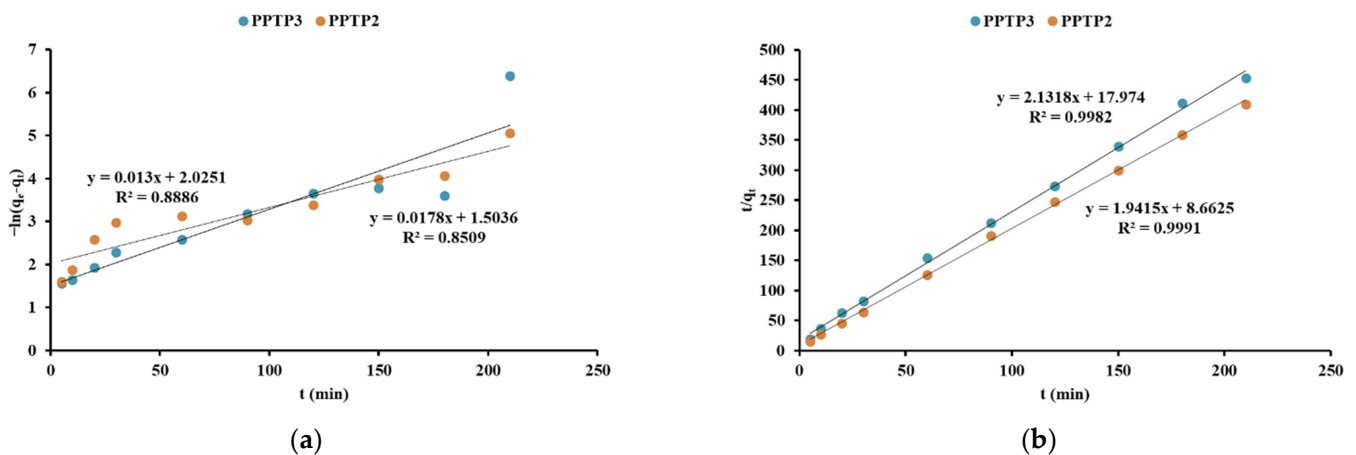


Figure 7. Kinetics of Li^+ ions ion exchange with the participation of PPTP2 and PPTP3 in the coordinates of the (a) pseudo-first- and (b) pseudo-second-order models ($C(\text{Li}^+) = 0.01 \text{ mol/L}$, $D = 10 \text{ g/L}$, room temperature).

Therefore, the ion-exchange chemical reaction between Li^+ ions and PPTP2 and PPTP3 was very likely the limiting stage of the process under study.

The experimental data were adapted to the Weber–Morris intraparticle diffusion model by plotting the square root of time ($t^{0.5}$) versus concentration (q_t) (Figure 8).

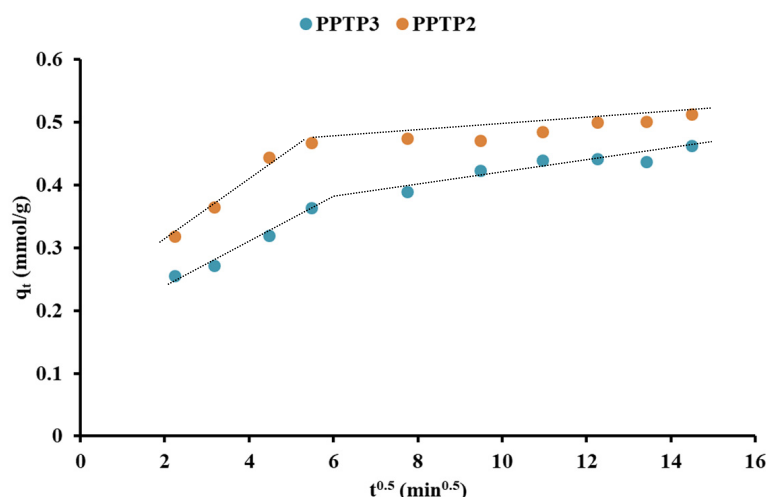


Figure 8. Kinetics of Li^+ ion exchange with the participation of PPTP2 and PPTP3 in the coordinates of the Weber–Morris model ($C(\text{Li}^+) = 0.01 \text{ mol/L}$, $D = 10 \text{ g/L}$, room temperature).

The graph did not pass through the origin, which means that diffusion within the PPTP particles was involved in the ion exchange process; however, it was not a step that controlled the rate of interaction, and it was not the only work mechanism. In addition, the graph had an initial linear section followed by a plateau. The initial section of the graph was attributed to the diffusion of ions through the solution to the outer surface of the ion exchanger or the diffusion of solute molecules in the boundary layer. The plateau was associated with the final equilibrium stage, when the processes inside the particle began to slow down due to the extremely low concentration of ions of the absorbed substance in the solution.

The values of the correlation coefficients R^2 and the kinetic constants were obtained from the slopes of the linear sections of the graphs, and the results are given in Table 2.

Table 2. Kinetic parameters of Li^+ ions ion exchange with the participation of PPTP2 and PPTP3.

Ion Exchanger	Pseudo-First Order Model			Pseudo-Second Order Model		
	R^2	q_e , mmol/g	k_1 , min^{-1}	R^2	q_e , mmol/g	k_2 , $\text{g}/(\text{mmol} \cdot \text{min})$
PPTP2	0.89	0.13	0.013	0.99	0.52	0.43
PPTP3	0.85	0.22	0.018	0.99	0.47	0.25

The calculated kinetic parameters of the pseudo-second-order model ($q_e = 0.47$ and 0.52 mmol/g) practically coincided with the experimental data ($q_e = 0.46$ and 0.52 mmol/g); therefore, it largely described the processes occurring in the system of protonated potassium polytitanate with an aqueous solution of lithium salt. This is why the mechanism of lithium extraction by protonated potassium polytitanates is an ion-exchange chemical reaction, which can cause strong binding and selectivity of the studied materials to lithium. Comparing the values of the sorption capacity from the pseudo-second-order kinetic model and the values of the cation-exchange capacity ($\text{CEC} = 3.42 \text{ mmol/g}$ and $\text{ECEC} = 0.42 \text{ mmol/g}$), it can be assumed that, over the studied period of time, the ion-exchange reaction predominantly occurred on the surface of PPTP and only partially involved the interlayer space. Therefore, there are prospects for improving their efficiency.

The most common materials for lithium extraction are protonated lithium manganates (Li-Mn-O) and titanates (Li-Ti-O). A comparison of their functional characteristics with protonated potassium polytitanate is presented in Table 3.

Table 3. Comparison of inorganic ion exchangers for lithium extraction.

Ion Exchanger	q , mmol/g	USD per kg	mmol per USD	Reference
Li–Mn–O	0.2–8.0	1500–5000	0.1–5.0	[18–30]
Li–Ti–O	0.9–14.0	1500–7500	0.1–9.0	[31–39]
PPTP2	0.52	20–30	17–26	this work

Despite the advantages of manganese and titanate spinels in terms of ion-exchange capacity, their high cost ultimately makes the method of ion-exchange extraction of lithium less economically viable and allows low-cost materials, such as protonated potassium polytitanate, to compete with them.

4. Conclusions

As a result of treatment in HCl solution at pH 2.0, 3.0, 4.0, 5.0, 6.0, or 7.0 of potassium polytitanate with a stoichiometry close to $K_2Ti_4O_9$, protonated samples were obtained with varying degrees of substitution of potassium ions for hydrogen ions, estimated from the data of X-ray fluorescence analysis. They were named PPTP2, PPTP3, PPTP4, PTKP5, PPTP6, and PPTP7. According to the results of X-ray phase analysis, protonated potassium polytitanates were characterized by an X-ray amorphous structure. The FTIR spectra of the study objects showed absorption bands associated with vibrations of the TiOH functional groups, the intensity of which varied depending on the degree of protonation. Among the studied samples, potassium polytitanates protonated at pH 2.0 and 3.0 had the highest efficiency in the extraction of lithium ions from an aqueous chloride solution. Using the pseudo-first- and pseudo-second-order kinetic models, as well as the Weber–Morris intraparticle diffusion model, the kinetics of ion exchange in the PPTP2 and PPTP3 systems with an aqueous solution of LiCl was studied. According to the best agreement between the experimental data and the pseudo-second-order kinetic model, it was established that the limiting stage of the ion-exchange process is a chemical reaction. The kinetic parameters were as follows: $q_e = 0.52$ mmol/g and $k_2 = 0.43$ for PPTP2; $q_e = 0.47$ mmol/g and $k_2 = 0.25$ for PPTP3.

Author Contributions: Conceptualization, M.V.; methodology, M.V.; software, M.V.; validation, M.V.; formal analysis, M.V. and A.G.; investigation, M.V., L.M. and V.R.; data curation, N.G.; writing—original draft preparation, M.V.; writing—review and editing, M.V. and N.G.; visualization, M.V.; supervision, M.V.; project administration, M.V.; funding acquisition, M.V. All authors have read and agreed to the published version of the manuscript.

Funding: This research was supported by the grant of the President of the Russian Federation, grant number MC-2204.2022.1.3.

Institutional Review Board Statement: Not applicable.

Data Availability Statement: Not applicable.

Acknowledgments: The authors thank Konstantin Kostin for performing the SEM measurements.

Conflicts of Interest: The authors declare no conflict of interest.

References

- Schlesinger, W.H.; Klein, E.M.; Wang, Z.; Vengosh, A. Global biogeochemical cycle of lithium. *Glob. Biogeochem. Cycles* **2021**, *35*, e06999. [[CrossRef](#)]
- Choi, H.-B.; Ryu, J.-S.; Shin, W.-J.; Vigier, N. The impact of anthropogenic inputs on lithium content in river and tap water. *Nat. Commun.* **2019**, *10*, 5371. [[CrossRef](#)] [[PubMed](#)]
- Lindsey, B.D.; Belitz, K.; Cravotta, C.A.; Toccalino, P.L.; Dubrovsky, N.M. Lithium in groundwater used for drinking-water supply in the United States. *Sci. Total Environ.* **2021**, *767*, 144691. [[CrossRef](#)] [[PubMed](#)]
- Thibon, F.; Metian, M.; Oberhänsli, F.O.; Montanes, M.; Vassileva, E.; Orani, A.M.; Telouk, P.; Swarzenski, P.; Vigier, N. Bioaccumulation of lithium isotopes in mussel soft tissues and implications for coastal environments. *ACS Earth Space Chem.* **2021**, *5*, 1407–1417. [[CrossRef](#)]

5. Aral, H.; Vecchio-Sadus, A. Toxicity of lithium to humans and the environment—A literature review. *Ecotoxicol. Environ. Saf.* **2008**, *70*, 349–356. [[CrossRef](#)]
6. Bolan, N.; Hoang, S.A.; Tanveer, M.; Wang, L.; Bolan, S.; Sooriyakumar, P.; Robinson, B.; Wijesekara, H.; Wijesooriya, M.; Keerthanan, S.; et al. From mine to mind and mobiles: Lithium contamination and its risk management. *Environ. Pollut.* **2021**, *290*, 118067. [[CrossRef](#)]
7. Melchor-Martínez, E.M.; Macias-Garbett, R.; Malacara-Becerra, A.; Iqbal, H.M.N.; Sosa-Hernández, J.E.; Parra-Saldívar, R. Environmental impact of emerging contaminants from battery waste: A mini review. *Case Stud. Chem. Environ. Eng.* **2021**, *3*, 100104. [[CrossRef](#)]
8. Mrozik, W.; Rajaeifar, M.A.; Heidrich, O.; Christensen, P. Environmental impacts, pollution sources and pathways of spent lithium-ion batteries. *Energy Environ. Sci.* **2021**, *14*, 6099–6121. [[CrossRef](#)]
9. Tanveer, M.; Hasanuzzaman, M.; Wang, L. Lithium in environment and potential targets to reduce lithium toxicity in plants. *J. Plant Growth Regul.* **2019**, *38*, 1574–1586. [[CrossRef](#)]
10. Ammari, T.G.; Al-Zu'bi, Y.; Abu-Baker, S.; Dababneh, B.; Gneamat, W.; Tahboub, A. The occurrence of lithium in the environment of the Jordan Valley and its transfer into the food chain. *Environ. Geochem. Health* **2011**, *33*, 427–437. [[CrossRef](#)]
11. Franzaring, J.; Schlosser, S.; Damsohn, W.; Fangmeier, A. Regional differences in plant levels and investigations on the phytotoxicity of lithium. *Environ. Pollut.* **2016**, *216*, 858–865. [[CrossRef](#)] [[PubMed](#)]
12. Kalinowska, M.; Hawrylak-Nowak, B.; Szymanska, M. The influence of two lithium forms on the growth, L-ascorbic acid content and lithium accumulation in lettuce plants. *Biol. Trace Elem. Res.* **2013**, *152*, 251–257. [[CrossRef](#)]
13. Lemaire, J.; Svecova, L.; Lagallarde, F.; Laucournet, R.; Thivel, P.X. Lithium recovery from aqueous solution by sorption/desorption. *Hydrometallurgy* **2014**, *143*, 1–11. [[CrossRef](#)]
14. Swain, B. Recovery and recycling of lithium: A review. *Sep. Purif. Technol.* **2017**, *172*, 388–403. [[CrossRef](#)]
15. Li, X.; Mo, Y.; Qing, W.; Shao, S.; Tang, C.Y.; Li, J. Membrane-based technologies for lithium recovery from water lithium resources: A review. *J. Membr. Sci.* **2019**, *591*, 117317. [[CrossRef](#)]
16. Meshram, P.; Pandey, B.D.; Mankhand, T.R. Extraction of lithium from primary and secondary sources by pre-treatment, leaching and separation: A comprehensive review. *Hydrometallurgy* **2014**, *150*, 192–208. [[CrossRef](#)]
17. Orooji, Y.; Nezafat, Z.; Nasrollahzadeh, M.; Shafiei, N.; Afsari, M.; Pakzad, K.; Razmjou, A. Recent advances in nanomaterial development for lithium ion-sieving technologies. *Desalination* **2022**, *529*, 115624. [[CrossRef](#)]
18. Chitrakar, R.; Makita, Y.; Ooi, K.; Sonoda, A. Selective uptake of lithium ion from brine by $H_{1.33}Mn_{1.67}O_4$ and $H_{1.6}Mn_{1.6}O_4$. *Chem. Lett.* **2012**, *41*, 1647–1649. [[CrossRef](#)]
19. Xiao, J.; Nie, X.; Sun, S.; Song, X.; Li, P.; Yu, J. Lithium ion adsorption–desorption properties on spinel $Li_4Mn_5O_{12}$ and pH-dependent ion-exchange model. *Adv. Powder Technol.* **2015**, *26*, 589–594. [[CrossRef](#)]
20. Sun, S.Y.; Song, X.; Zhang, Q.H.; Wang, J.; Yu, J.G. Lithium extraction/insertion process on cubic Li-Mn-O precursors with different Li/Mn ratio and morphology. *Adsorption* **2011**, *17*, 881–887. [[CrossRef](#)]
21. Xiao, G.; Tong, K.; Zhou, L.; Xiao, J.; Sun, S.; Li, P.; Yu, J. Adsorption and desorption behavior of lithium ion in spherical PVC-MnO₂ ion sieve. *Ind. Eng. Chem. Res.* **2012**, *51*, 10921–10929. [[CrossRef](#)]
22. Bajestani, M.B.; Moheb, A.; Dinari, M. Preparation of lithium ion-selective cation exchange membrane for lithium recovery from sodium contaminated lithium bromide solution by electrodialysis process. *Desalination* **2020**, *486*, 114476. [[CrossRef](#)]
23. Zhan, H.; Qiao, Y.; Qian, Z.; Li, J.; Wu, Z.; Hao, X.; Liu, Z. Manganese-based spinel adsorbents for lithium recovery from aqueous solutions by electrochemical technique. *J. Ind. Eng. Chem.* **2022**, *114*, 142–150. [[CrossRef](#)]
24. Zhang, Q.H.; Li, S.P.; Sun, S.Y.; Yin, X.S.; Yu, J.G. $LiMn_2O_4$ spinel direct synthesis and lithium ion selective adsorption. *Chem. Eng. Sci.* **2010**, *65*, 169–173. [[CrossRef](#)]
25. Ma, L.W.; Chen, B.Z.; Chen, Y.; Shi, X.C. Preparation, characterization and adsorptive properties of foam-type lithium adsorbent. *Microporous Mesoporous Mater.* **2011**, *142*, 147–153. [[CrossRef](#)]
26. Liu, L.; Zhang, H.; Zhang, Y.; Cao, D.; Zhao, X. Lithium extraction from seawater by manganese oxide ion sieve $MnO_2 \cdot 0.5H_2O$. *Colloids Surf. A Physicochem. Eng. Asp.* **2015**, *468*, 280–284. [[CrossRef](#)]
27. Shi, X.; Zhou, D.; Zhang, Z.; Yu, L.; Xu, H.; Chen, B.; Yang, X. Synthesis and properties of $Li_{1.6}Mn_{1.6}O_4$ and its adsorption application. *Hydrometallurgy* **2011**, *110*, 99–106. [[CrossRef](#)]
28. Xiao, J.L.; Sun, S.Y.; Wang, J.; Li, P.; Yu, J.G. Synthesis and adsorption properties of $Li_{1.6}Mn_{1.6}O_4$ spinel. *Ind. Eng. Chem. Res.* **2013**, *52*, 11967–11973. [[CrossRef](#)]
29. Sun, S.Y.; Xiao, J.L.; Wang, J.; Song, X.; Yu, J.G. Synthesis and adsorption properties of $Li_{1.6}Mn_{1.6}O_4$ by a combination of redox precipitation and solid-phase reaction. *Ind. Eng. Chem. Res.* **2014**, *53*, 15517–15521. [[CrossRef](#)]
30. Chitrakar, R.; Kanoh, H.; Makita, Y.; Miyai, Y.; Ooi, K. Synthesis of spinel-type lithium antimony manganese oxides and their Li⁺ extraction/ion insertion reactions. *J. Mater. Chem.* **2000**, *10*, 2325–2329. [[CrossRef](#)]
31. Shi, X.C.; Zhang, Z.B.; Zhou, D.F.; Zhang, L.F.; Chen, B.Z.; Yu, L.L. Synthesis of Li⁺ adsorbent (H_2TiO_3) and its adsorption properties. *Trans. Nonferrous Met. Soc. China* **2013**, *23*, 253–259. [[CrossRef](#)]
32. Chitrakar, R.; Makita, Y.; Ooi, K.; Sonoda, A. Lithium recovery from salt lake brine by H_2TiO_3 . *Dalton Trans.* **2014**, *43*, 8933–8939. [[CrossRef](#)] [[PubMed](#)]
33. Zhang, L.; Zhou, D.; He, G.; Wang, F.; Zhou, J. Effect of crystal phases of titanium dioxide on adsorption performance of H_2TiO_3 -lithium adsorbent. *Mater. Lett.* **2014**, *135*, 206–209. [[CrossRef](#)]

34. He, G.; Zhang, L.; Zhou, D.; Zou, Y.; Wang, F. The optimal condition for H₂TiO₃–lithium adsorbent preparation and Li⁺ adsorption confirmed by an orthogonal test design. *Ionics* **2015**, *21*, 2219–2226. [[CrossRef](#)]
35. Tang, D.; Zhou, D.; Zhou, J.; Zhang, P.; Zhang, L.; Xia, Y. Preparation of H₂TiO₃–lithium adsorbent using low-grade titanium slag. *Hydrometallurgy* **2015**, *157*, 90–96. [[CrossRef](#)]
36. Lawagon, C.P.; Nisola, G.M.; Mun, J.; Tron, A.; Torrejos, R.E.C.; Seo, J.G.; Chung, W.J. Adsorptive Li⁺ mining from liquid resources by H₂TiO₃: Equilibrium, kinetics, thermodynamics, and mechanisms. *J. Ind. Eng. Chem.* **2016**, *35*, 347–356. [[CrossRef](#)]
37. Limjuco, L.A.; Nisola, G.M.; Lawagon, C.P.; Lee, S.P.; Seo, J.G.; Kim, H.; Chung, W.J. H₂TiO₃ composite adsorbent foam for efficient and continuous recovery of Li⁺ from liquid resources. *Colloids Surf. A Physicochem. Eng. Asp.* **2016**, *504*, 267–279. [[CrossRef](#)]
38. Wang, S.; Li, P.; Cui, W.; Zhang, H.; Wang, H.; Zheng, S.; Zhang, Y. Hydrothermal synthesis of lithium-enriched β-Li₂TiO₃ with an ion-sieve application: Excellent lithium adsorption. *RSC Adv.* **2016**, *6*, 102608–102616. [[CrossRef](#)]
39. Zhang, L.; Zhou, D.; Yao, Q.; Zhou, J. Preparation of H₂TiO₃-lithium adsorbent by the sol-gel process and its adsorption performance. *Appl. Surf. Sci.* **2016**, *368*, 82–87. [[CrossRef](#)]
40. Machida, M.; Ma, X.W.; Taniguchi, H.; Yabunaka, J.I.; Kijima, T. Pillaring and photocatalytic property of partially substituted layered titanates, Na₂Ti_{3-x}M_xO₇ and K₂Ti_{4-x}M_xO₉ (M = Mn, Fe, Co, Ni, Cu). *J. Mol. Catal. A Chem.* **2000**, *155*, 131–142. [[CrossRef](#)]
41. Yang, J.; Li, D.; Wang, X.; Yang, X.; Lu, L. Study on the synthesis and ion-exchange properties of layered titanate Na₂Ti₃O₇ powders with different sizes. *J. Mater. Sci.* **2003**, *38*, 2907–2911. [[CrossRef](#)]
42. Yuan, X.; Li, W.; Liu, X. Comparative Study of Proton Exchange in Tri- and Hexatitanates: Correlations between Stability and Electronic Properties. *Inorg. Chem.* **2022**, *61*, 3918–3930. [[CrossRef](#)] [[PubMed](#)]
43. Mori, M.; Kumagai, Y.; Matsunaga, K.; Tanaka, I. First-principles investigation of atomic structures and stability of proton-exchanged layered sodium titanate. *Phys. Rev. B* **2009**, *79*, 144117. [[CrossRef](#)]
44. Gorokhovskiy, A.V.; Escalante-Garcia, J.I.; Sanchez-Monjaras, T.; Gutiérrez-Chavarría, C.A. Synthesis of potassium polytitanate precursors by treatment of TiO₂ with molten mixtures of KNO₃ and KOH. *J. Eur. Ceram. Soc.* **2004**, *24*, 3541–3546. [[CrossRef](#)]
45. Marković, M.; Daković, A.; Rottinghaus, G.E.; Petković, A.; Kragović, M.; Krajišnik, D.; Milić, J. Ochratoxin A and zearalenone adsorption by the natural zeolite treated with benzalkonium chloride. *Colloids Surf. A Physicochem. Eng. Asp.* **2017**, *529*, 7–17. [[CrossRef](#)]
46. Kragović, M.; Daković, A.; Sekulić, Ž.; Trgo, M.; Ugrina, M.; Perić, J.; Gatta, G.D. Removal of lead from aqueous solutions by using the natural and Fe (III)-modified zeolite. *Appl. Surf. Sci.* **2012**, *258*, 3667–3673. [[CrossRef](#)]
47. Ming, D.W.; Dixon, J.B. Quantitative determination of clinoptilolite in soils by a cation-exchange capacity method. *Clays Clay Miner.* **1987**, *35*, 463–468. [[CrossRef](#)]
48. Al-Gebory, L.; Mengüç, M.P. The effect of pH on particle agglomeration and optical properties of nanoparticle suspensions. *J. Quant. Spectrosc. Radiat. Transf.* **2018**, *219*, 46–60. [[CrossRef](#)]
49. Marthi, R.; Asgar, H.; Gadikota, G.; Smith, Y.R. On the structure and lithium adsorption mechanism of layered H₂TiO₃. *ACS Appl. Mater. Interfaces* **2021**, *13*, 8361–8369. [[CrossRef](#)]